Pisco Med Publishing

Insight - Material Science, 2019, 2(1) doi: 10.18282/ims.v2i1.180

Article

# Staircase-Like Crack Progression Due to Hydrogen Embrittlement of Cold-Worked Steel Strand

Joseph Rogelio Fernandez

*Saint Petersburg College, 2465 Drew St, Clearwater, Florida 33765, USA*

***ABSTRACT***

Stressed carbon steel strand in an ungrouted duct susceptibility to pitting corrosion is low due to surface corrosion, but susceptibility of steel strand to Hydrogen Embrittlement (HE) can increase under those conditions.

The HE will facilitate crack growth within the strand. Various crack propagation mechanisms, such as longitudinal splitting and shear-cracking, have been shown as possible strand failure mechanisms by themselves in strand, but this may not be true in stressed strand in piles that has been embrittled by Hydrogen and without pre-cracking (Cracks initiating from stress concentrations naturally rather than with notching). Concentration measurements were performed to determine the level of Hydrogen involved in the embrittlement.

Results indicate that the fracture mechanism differs from shear cracking or longitudinal splitting alone as previously shown, but is a multi-step process of crack propagation starting perpendicular to stress, followed by variations of inter-lamellae longitudinal splitting at brittle region of lamellae and shear cracking at breaks in the lamellae. This process results in the crack following a "staircase" progression, and finally leading to ductile overload once cross-section has been significantly reduced. This fracture mechanism was also shown to be valid whether the strand was stressed by bending or mult-axially by stressing through a duct.

***KEYWORDS:*** Mechanical; Creep and stress rupture; Thermomechanical Processing; Failure analysis; Corrosion and wear

**Received:** Nov. 20th, 2018 **Accepted:** Dec. 26th, 2018 **Online:** Dec. 11th, 2019

## Nomenclature

AISI - American Iron and Steel Institute.

$C_H$ - Outgassed Hydrogen Concentration, ppmw.

$L_R$ - Pressure leak rate in the system.

$m_{STEEL}$ - Mass of the steel specimen in grams.

$MW_H$ - Molecular Weight of Hydrogen, 2.016 g/mol.

$P_I$ - Initial pressure of the system.

$P_o$ - Total pressure change (in Torr) over the entire outgassing measurement.

P(t) - Pressure corresponding to the amount of hydrogen outgassed into the chamber volume V.
$P_L(t)$ - Pressure in system due to leak rate at time t, $L_R$ * t.
q - Constant used to convert the pressure from Torr to Pa, 133.322 Torr/Pa.R - Gas Constant 8.314 J/mol-K.
t - Time since the start of the experiment.
$t_o$ - Time at which the specimen achieves the outgassing temperature.
T - Absolute room temperature in K (assumed to be 298 K (Celsius)).
V - Volume of the system in $cm^3$.τ - Time constant of outgassing system.
ΔP(t) - Change in pressure corresponding to the amount of hydrogen outgassed into the chamber volume V.

# 1. Introduction

Currently, carbon steel is used in post-tension applications, where several instances of post-tension brittle strand failure have occurred, including instances due to being left ungrouted[1]. A relationship between hydrogen concentrations of exposed specimen to hydrogen concentrations of specimens charged with hydrogen to point of fracture will gauge susceptibility of HE of stressed strands used in post-tensioning.

The exact failure mechanism of strand under stress failing due to HE is not well understood. Various mechanisms, such as longitudinal splitting or shear-cracking, have been used to detail cold-worked steel embrittlement but may not be the exact case in stressed strand wire[2].

Hydrogen Embrittlement (HE) can affect alloys that actively corrode (due to surface reactions with salt and/or water on the surface of the strand). HE occurs when atomic hydrogen has entered the metallic alloy bulk and built up to a critical concentration (which can be very small, hence easily reached). On application of sufficiently high tensile stress the hydrogen experiences preferential transport (often by diffusion or dislocation motion) to regions of stress concentration, where cracks develop and propagate. The adverse effect has been explained alternatively by the phenomena of Hydrogen Induced Decohesion (HID), Hydrogen Enhanced Localized Plasticity (HELP), and Adsorption Induced Dislocation Emission (AIDE)[3-5].

Hydrogen becomes naturally available at a wet steel surface when cathodic, hydrogen evolution reactions take place there as part of corrosion processes. Corrosion reactions can occur in humid air, distilled water, acid environments, neutral environments, or alkaline environments[6]. The cathodic reaction removes the electrons that are created by the anodic reaction (metal dissolution, Fe -→ Fe+2 + 2e-) on the steel surface. The cathodic reaction is often oxygen reduction, expressed as ½ O2 + H2O + 2e- → 2OH- if the water solution is neutral or alkaline, or H+ + e → ½ H2 (hydrogen ion reduction) if acidic. If oxygen is depleted and the solution is neutral or alkaline, the reduction reaction consists of direct water decomposition, H2O + e- → ½ H2 + OH-[7].

Both hydrogen evolution reactions are written above as forming hydrogen molecules. However, those reactions are known to involve intermediate steps where atomic hydrogen is formed first as a surface adsorbate which then recombines as H2[8]. Most of the evolved hydrogen ends up as H2[8] which are too large to enter into the interstitial sites of the crystal structure of the steel, and thus bubble off the surface into the electrolyte. Atomic hydrogen is small enough in size to become an interstitial atom in the steel (entering the tetrahedral sites of the lattice), so a fraction (e.g., 1/100) of the total hydrogen produced by the cathodic reactions actually enters the steel bulk[8].

Although the fraction of H penetrating the steel is small, the amount of hydrogen required to initiate HE at a location of stress concentration is as noted earlier equally very small. This can be attributed to the smaller interstitial space of the tetrahedral sites and the inability for much expansion before the bonds are weakened[8]. A concentration of ~0.03 ppm of diffusible hydrogen is sufficient to initiate HE in post tensioning steel strand[2]. It is shown (in Figure 13 of Ref 9) that the amount of hydrogen permeation flux (indicative of the rate of penetration of H into the steel) is 5.15e-13 mol/cm2-sec for the case of minor surface corrosion cathodic reations on strand steel, for example those resulting in a

corrosion rate of only 1uA/cm2 , which corresponds to corrosion rates of only ~10 um/y[3,9]. Therefore, while the general corrosion rate is small, the amount of hydrogen created and transported to stress concentrations can be more than enough to embrittle the material.

An important factor in the failure mechanism of the cold-worked, pearlitic steel strands is that the lamellae is stretched in the drawing direction which tends to separate the layers so that there are "gaps" in the ferritic layers. Also, the interlamellae spacing is reduced from the typical 330 nm[2] to 220 nm for the carbon steel strands tested. The gaps in the lamellae are filled with cementite (from the interlamellae space that was reduced), which tends to be more brittle than the ferritic layers. Due to these gaps filled with cementite, when a crack begins propagating in-between the ferritic layers and comes to a "gap", the crack may turn perpendicular to the layer axis and move to the next lower layer. This propagation path can lead to a staircase pattern, splitting portions of the lamellae apart along the way while then shear cracking occurs, turning the crack propagation perpendicular again. Eventually, this combination of inter-lamellae splitting and shear cracking progression in a staircase pattern can lead to a loss of bonded cross-section. When the still bonded cross-section is reduced enough, ductile overload can occur.

# 2. Materials and methods

## 2.1 Material used in post-tension applications

The material tested was a heavily cold-worked pearlitic AISI 1080 7-wire steel strand. The strand diameter is nominally ~1.27 cm and has estimated yield strength of 1.86 GPa. The elemental composition is 0.6 % Manganese, 0.75% Carbon, 0.05% Sulfur, 0.04% Phosphorous and with the balance being Iron (~98.56%).

## 2.2 Hydrogen concentration measurement method

The procedure for the measurement of the hydrogen concentration in a wire specimens consisted of the outgassing of hydrogen in a vacuum system. **Figure 1** and **Figure 2** show a diagram and a photograph of the vacuum system setup, respectively.

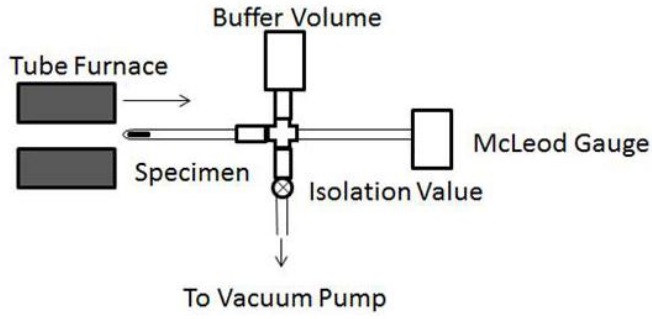


**Figure 1.** Diagram of hydrogen concentration measurement setup

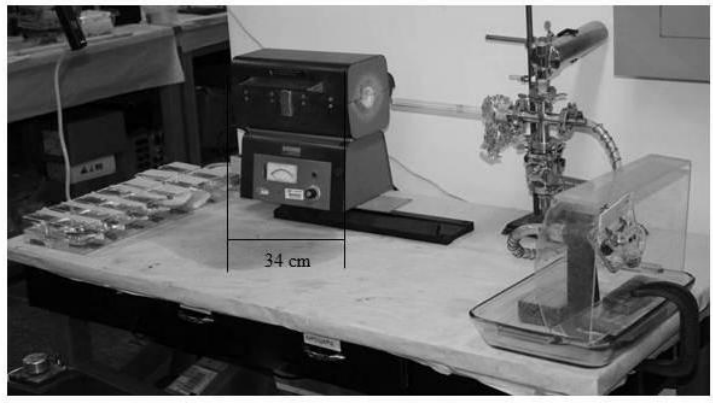


**Figure 2.** Hydrogen concentration measurement setup

Specimens for this test consisted of a set of four 5.08 cm pieces from the outer wires for each strand. Each piece was glass-bead blasted to ensure that there was no surface rust which during outgassing can produce water vapor and falsely increase the hydrogen concentration reading. Then the pieces were placed together in a 1.27 cm internal diameter quartz tube, sealed at the end closest to the specimens and with the other end connected to the vacuum system. The vacuum system was then sealed and pumped down to about 0.05 Torr with a mechanical vacuum pump. A valve was closed isolating the pump from the rest of the sealed vacuum system, which had a total volume of 824 $cm^3$. Measurements of the system pressure were taken using a McLeod gauge every minute to establish the value of the leaking rate. After five minutes, a tube furnace set at a temperature of 753 K (Celsius) was slid over the quartz tube end containing the specimen; the rest of the system remaining at room temperature. Measurements of the system pressure were taken every minute for at least another 35 minutes. The pressure gauge data was corrected for parallax and point of view errors using electronic camera photos taken at each measurement. A photo pixel counting program was used to accurately conduct those corrections.

The temperature of 753 K (Celsius) was chosen as a temperature at which only hydrogen would be expected to be outgassed from the specimen in the time frame of the tests (higher temperature can lead to the outgassing of carbon monoxide or carbon dioxide which can lead to the creation of methane in the system). The pressure versus time data were plotted as exemplified in Figure 3.

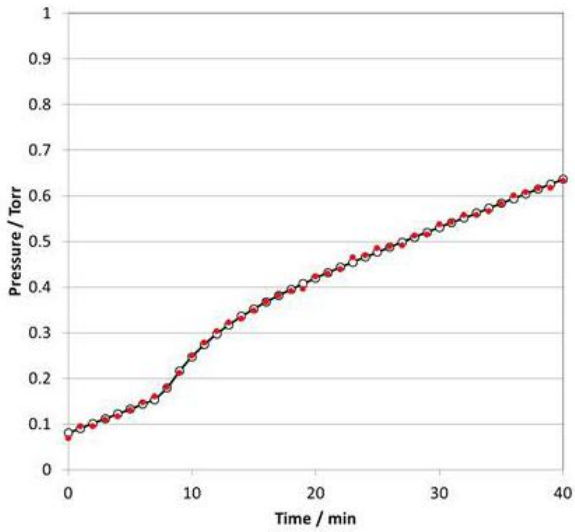


**Figure 3.** Hydrogen concentration calculations from measurements example for specimen 89a. Parameter fit Values:$t_o$ = 7.53 Minutes, $P_o$ = 0.08 Torr, = 3.99 Minutes, $\tau$ = 0.01 Torr/ Minute, hydrogen concentration value 0.55 ppmw. Red symbols: Data; Black symbols: Model fit

The results showed an initial pre-heating increase in pressure corresponding to the leak rate of the system, an intermediate period where the bulk of the outgassing took place, and a terminal stage of return toward the baseline leak rate. The increase in pressure associated with outgassing was assumed on first approximation to follow single time constant $\tau$ kinetics of the form

$$\Delta P(t) = P_o (1-\exp^{-(t-to)/} \tau) \quad (1)$$

where

P(t) is the pressure corresponding to the amount of hydrogen outgassed into the chamber volume V,

t is the time since the start of the experiment,

$t_o$ is the time at which the specimen achieves the outgassing temperature,

$\tau$ is the time constant of outgassing system,

and $P_o$ is the total pressure change (in Torr) over the entire outgassing measurement.

The increase is a function of effective time (t-to) since the moment when the specimen achieved the outgassing temperature, and for t < to, ΔP(t) is assigned a value of zero. Per the above, at any given time the total pressure is then assumed to be given by

$$P_{TOTAL}(t) = P_I + P_L(t) + \Delta P(t) \quad (2)$$

where
$L_R$ is the pressure leak rate in the system,
$P_L(t) = L_R * t$,
$P_I$ is the initial pressure

The pressure versus time data was then compared with the $P_{TOTAL}(t)$ modeled per Equation (2) with the values of to, τ, $L_R$, $P_I$ and Po as adjustable parameters. The sum of the squared differences between model and measured data was treated as a minimization variable. The values of the parameters, in particular Po, for minimum condition were then obtained by use of the SOLVER function in an Excel spreadsheet. The value of Po was used, assuming ideal gas behavior, to estimate the outgassed hydrogen concentration $C_H$ which with the choice of units indicated below is in weight parts per million, (ppmw) by:

$$C_H = (MW_H * P_o * V) / (q * m_{STEEL} * R * T) \quad (3)$$

where
$MW_H$ is the molecular weight of Hydrogen, 2.016 g/mol,
$m_{STEEL}$ is the mass of the steel specimen in grams,
R is the gas constant 8.314 J/mol-K,
V is the volume of the system in $cm^3$,
T is the absolute room temperature in K (assumed to be 298 K (Celsius)),
and q is a constant used to convert the pressure from Torr to Pa, 133.322 Torr/Pa.

The values of the other parameters were used only to verify plausibility of the outcome. $L_R$ was found to be close to the visually estimated initial leak rate; to was found to be in the order of two minutes after furnace move, consistent with the expected warm up time of the specimen; τ was in the order of several minutes consistent as well with the expected diffusivity of Hydrogen at the operating temperature and typical diffusivity values[2], and $P_I$ was close to the observed initial pressure.

An uncertainty analysis of the test outcome was performed by first taking the pressure data for t > 20 min (corresponding to the terminal pressure-time slope where pressure increases quite linearly with time) from six different randomly selected specimens. Then for each specimen the data were linearly de-trended and the standard deviation was calculated. That standard deviation is thus representative in each case of the random scatter of the pressure data around a nominal true value at a given time. The average of those standard deviations, $\sigma_a$ = 0.006 Torr, was then calculated as an overall typical value for these experiments. Simulated data sets were then created by constructing ideal pressure evolution tables at 1 minute intervals using Equations (1-3) with parameters $t_o$ = 6 minutes, τ= 6 minutes, $L_R$ = 0.01 Torr /minute , $P_I$ = 0.05 Torr, $m_{STEEL}$ = 20 g, V = 700 cc, T = 298 K (Celsius) and Po corresponding to $C_H$ values ranging from 0.01 to 1 ppmw. The ideal pressure value for each time in each set was then added an individually randomized simulated normally-distributed scatter contribution with standard deviation $\sigma_a$. The procedure was repeated 10 times for each set, effectively simulating the data of a group of 10 replicate experiments. The simulated data sets were then processed by the same program used to interpret the laboratory data, yielding a group of estimated $C_H$ values. The standard deviation of that group was then calculated and the result was named $\sigma C_H$. The entire procedure was performed twice to obtain a richer field of simulated results. The value of $\sigma C_H$ was found to be in the order of 0.04 ppmw, and to not vary systematically with the initially assumed value of $C_H$ within the 2-order of magnitude range assumed above. The value of 0.04 ppmw was consequently deemed to be the approximate detection limit and representative of the random error of the test method.

## 2.3 Hydrogen charging method

A set of 144 strands were exposed to various test conditions, including salt spray and wetting, while under stress. These exposed specimens were considered charged with hydrogen by the surface corrosion reactions undergone in post-tension ducts while ungrouted. In addition to those specimens, additional specimens were electrochemically charged to the point of failure to use as a reference concentration value. Testing of previously unexposed strand specimens for HE susceptibility was performed using hydrogen charging with a solution of 875 mL of DI water, 125 mL of Sulfuric Acid ($H_2SO_4$), and 0.5 grams of Antimony Trioxide ($Sb_2O_3$) [as a hydrogen recombination poison] while cathodic polarization to about 0.05 A/cm$^2$ occurred at room temperature 298 K (Celsius). The setup is shown in **Figure 4**.

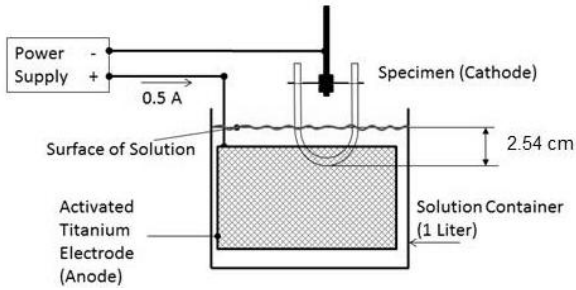


**Figure 4.** Diagram of hydrogen charging setup with variable power source

The stressing of the specimens while being charged was implemented by bending the specimens into a "U" shape and maintaining that shape using a pre-drilled brace plate, to create conditions that can lead to HE. Details of the bending procedure are given by[10]. Bending the specimens 180° deformed them plastically as well as elastically, ensuring the yield strength of the material is exceeded, and possibly increasing the sensitivity to HE. The specimens were initially charged for as much as 24 hours at lower polarization (0.01 A/cm$^2$ ), but shorter charging times while ensuring hydrogen charging sufficient to induce delayed failure was desired. It was discovered through numerous iterations, that delayed failure due to HE could be routinely achieved by charging the specimens for as little as 25 minutes at 0.05 A/cm$^2$. This combination was chosen for the subsequent tests as it reduced the testing time and was sufficient to initiate HE-induced cracking and mechanical failure as desired.

## 2.4 Stressed strand charging

A specific issue in relating of the U-bent specimen failures to possible stressed strand failures was raised during this research. The stresses applied to the U-bent wire specimens are at a level well above the yield strength, but the stress level applied to the stress strands is well below the yield strength in comparison. The stresses applied by the U-bend are a combination of tensile (in the outer portion of the bend) and compression (in the inner portion of the bend) stresses, while the stressing of strands in a pile are of a multi-axial nature. Therefore, three strands were tested in which one strand was stressed to the same levels of stress as that applied during the set of 144 stress strand testing (nominal stress of 243.9 ksi, or 0.90 $f_{pu}$). Load cells (four load cells to allow for duplication of data) were attached to record the stress loads on the strand over time. The charging setup consisting of a sponge wetted with the hydrogen charging solution used in the previous section connected to the center region of the stressed strand through the vent port. This region of the strand was in electrical contact (through the charging solution, as an electrolyte, in the sponge) with a activated titanium mesh on the outside of the sponge. The mesh was connected to the positive terminal of the power supply making the mesh the anodic connection point, while a conductive clamp was attached to another point on the strand (outside of the pile duct) to act as the cathodic connection point. A power supply was use to charge the strand at 0.05 A/cm$^2$ for 25 minutes. Because the hydrogen charging solution only contacted at the point where the sponge was, and that connection was to the positive terminal on the power supply, the strand would be negatively charged as is done during cathodic protection. Therefore, hydrogen would be generated as was shown previously. Specifically, hydrogen charging occurred at the location only on which the wetted sponge was placed on the strand.

# 3. Results and discussion

The hydrogen concentration measurements for unexposed (to salt and water), exposed and purposely charged specimens are shown in **Figure 5**[11].


**Figrure 5.** Hydrogen concentration test results

It is emphasized that the hydrogen concentrations values below ~0.04 ppmw (roughly in the order of the sensitivity of the test) are nominal indications of the experimental test curve fitting procedure and not distinguishable from zero content. Starting for the left of the chart, the first set of four values are for strand specimens cut directly from the spool and kept in an air conditioned environment until tested, showing essentially no detectable hydrogen content with the test as performed. The next set of data shows the hydrogen concentrations of five specimens electrochemically charged in the laboratory using the hydrogen charging method described earlier. The "Individually Charged" and "Together Charged" specimens were charged in the unstressed condition. The Bent/Broken specimen was charged in the stressed condition for 25 minutes (a condition that resulted in hydrogen-induced cracking as shown later). All the charged specimens showed concentrations in the order or 0.5 to 2 ppmw hydrogen, clearly much higher than that of the as-received control specimens.

The remaining specimens were cut out of field-exposed strands in conditions representative of the variety of exposure regimes used. Specimens are designated by a code block indicating the exposure condition (e.g. CWS2 means Closed Wet Salted, 2-weeks) plus the specimen ID. While the data set is limited and shows significant variability, some trends may be discerned from the results. Most importantly, the measured hydrogen concentrations of the specimens exposed to the most severe regime (salted and wet environment) were on average relatively close to the concentration of the hydrogen-charged specimens, which exploratory tests indicate are prone to hydrogen embrittlement in severe bending regimes (see next section). In contrast, the specimens exposed to the mildest conditions in the set from the point of view of visual appearance indicated earlier on (open unsalted) had concentrations measurement values close to those of the unexposed controls.

The most conclusive results have been with specimens charged to conditions that resulted in measured hydrogen concentrations between ~0.5 to 2 ppmw. When those specimens were charged in the U-bend configuration, several instances of spontaneous fracture took place. In some instances near the end of the 25-minute charging period incipient cracks were noted, followed by spontaneous full fracture within about 2.5 hours. The phenomenon has the typical

characteristics of delayed-cracking hydrogen embrittlement and the hydrogen levels are consistent with those observed elsewhere to have promoted hydrogen embrittlement in strand steel[2].

The exact failure mechanism for stressed cold-worked, pearlitic steel strand under tension follows a multi-step process (as shown in parts A through E of **Figure 6**[11]). An example of this failure pattern is shown in **Figure 7**.

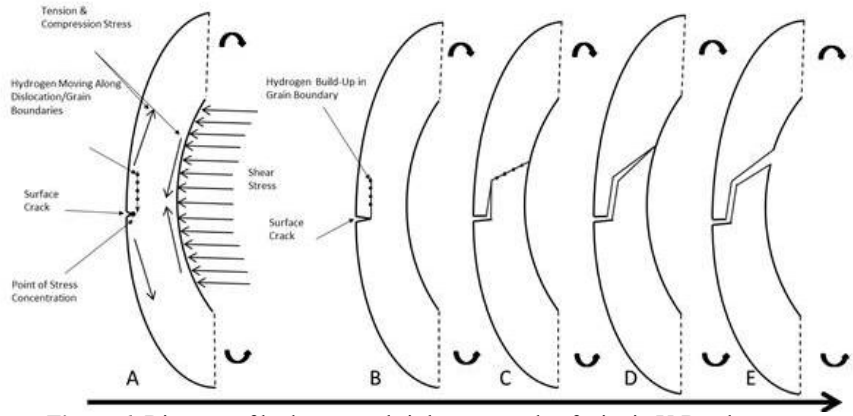


**Figure 6.** Diagram of hydrogen embrittlement mode of wire in U-Bend test

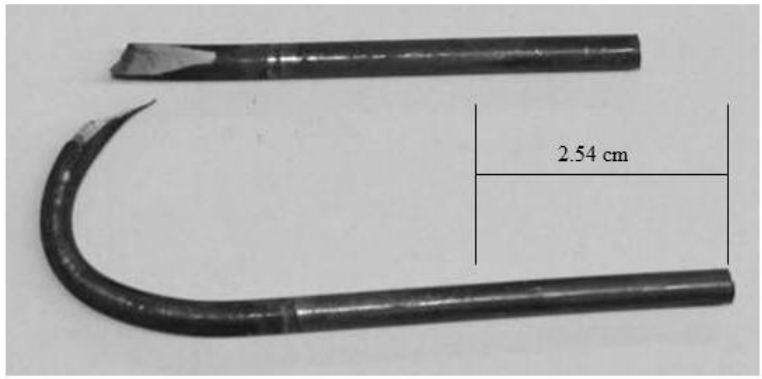


**Figure 7.** U-Bend specimen failed due to delayed failure hydrogen embrittlement

Initially, a crack at the surface propagates perpendicular to the stress direction (part B of Figure 6), and then reaches a lamellae at which point, the separation of the layers occurs (part C of Figure 6 and shown by the split in Figure 8). As the lamellae are not one continuous layer throughout the material, the cracking propagates through spaces in the layers in a staircase manner through the cross-section of the wire (as shown in Figure 9). Eventually, the cross-section is reduced by the breaking of bonds to the point of ductile overload.


**Figure 8.** Failed specimen showing delay failure and splitting due to crack propagation

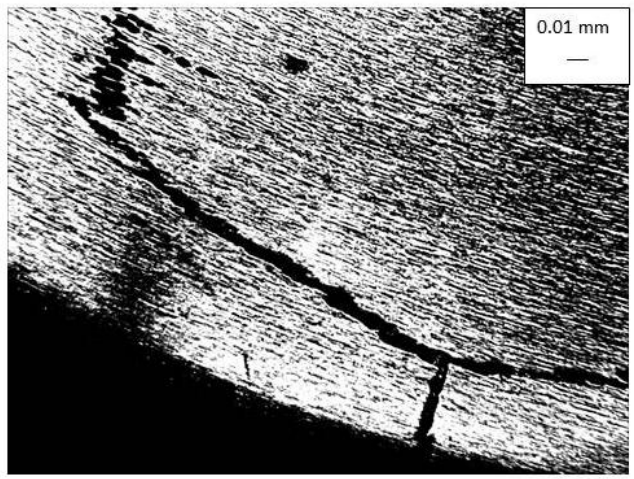


**Figure 9.** (Etched) Metallography of cracks developing into breaks

**Figure 10**, **Figure 11**, and **Figure 12** illustrate the fracture morphology and are examples full fracture and initial cracking progression. **Figure 10** shows the point at the surface in which the crack nucleates from (as indicated by the arrow) as well as the initiation point of the splitting of the lamellae layers. **Figure 11** displays the separation of the lamellae layers (indicated by the arrow) by crack propagated from the initial surface crack. **Figure 12** contains an example of the staircase pattern of crack propagation along point of voids in the lamellae layers (as indicated by the arrow). In the U-Bend configuration used, brittle cracks initiate normal to the tensile stress in the outer fibers of the bent specimen and then quickly transition into a longitudinal splitting then a shear mode through the lamellae that runs parallel to the drawing direction, favoring the cementite-ferrite interfaces. The crack progress shifts from shear cracking to longitudinal splitting and back leading to the staircase crack propagation pattern.

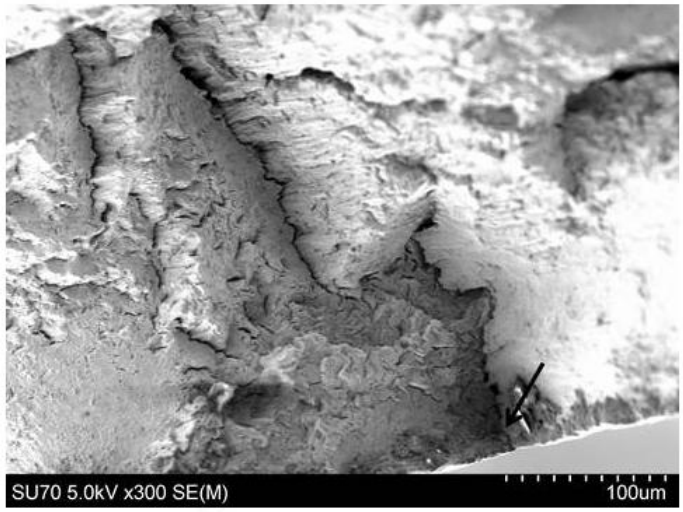


**Figure 10.** SEM of surface cracks developing into inter-lamellae splitting

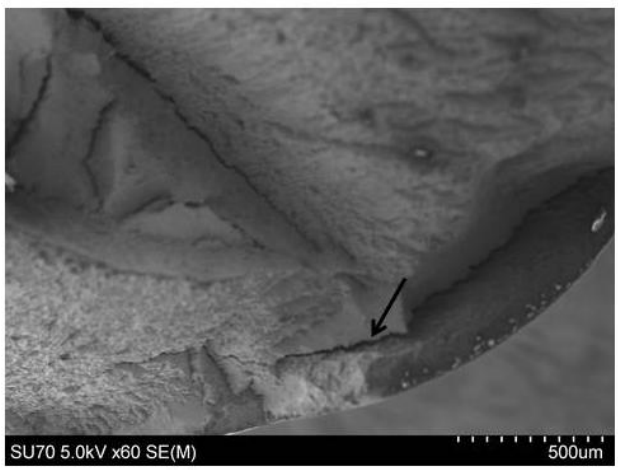


**Figure 11.** Increased magnification SEM of inter-lamellae splitting

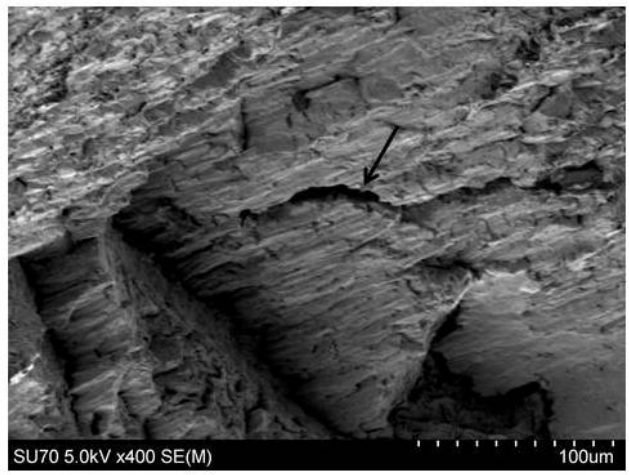


**Figure 12.** SEM of cracking following staircase pattern through lamellae

It is emphasized that these U-bend tests involve a very severe level of stress, a loading configuration quite different from the straight tensile loading encountered in a tendon, and a very high cathodic current density that promotes the development of similarly enhanced transient hydrogen concentrations near the metal surface.

Similar fracture patterns were also found in the three strands stressed multi-axially under more nominal loads indicating that the form of stressing and the stress level as compared to the yield strength were not factors in the crack propagation pattern. The load cell data is shown in Figure 13 and indicates the time at which wires in the strand failed by the decrease in the load on the strand. All three strands showed a decrease in the load between 0.5 and 1.75 hours after charging ended (charging ended ~0.5 hours after the strand was stressed the load required).

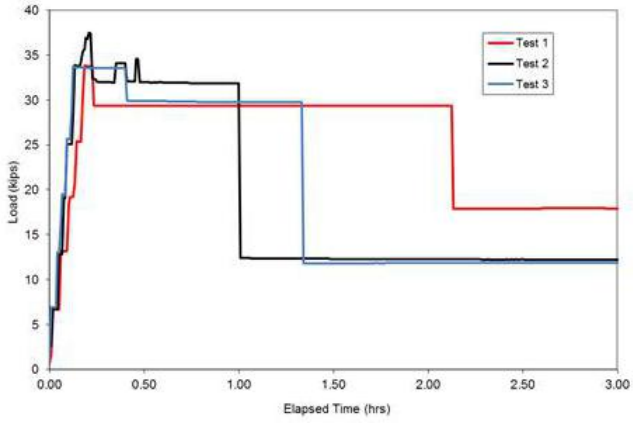


**Figure 13.** Load cell measurements from stressed and charged strands

**Figure 14** and **Figure 15** show the fractured specimens with cracks following the multi-step staircase crack propagation process. Overall, the combination of longitudinal splitting and shear cracking leads to a fracture pattern with the outer portion of the specimen break as a ledge, and the rest of the cross-section as a jagged break pattern to overload failure. **Figure 15** shows two pieces of the same fracture placed together to show both halves. This figure shows in detail the entire fracture progression, starting with vertical crack growth (1), leading to shear cracking (2), followed by longitudinal splitting (3), which leads to a jagged pattern of the combination of shear cracking and longitudinal splitting (4), and finally overload failure (5).

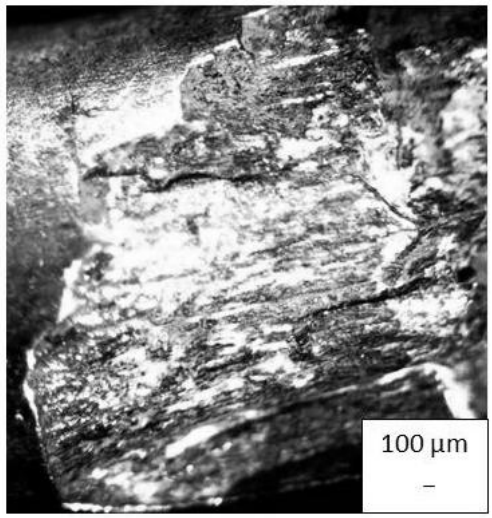


**Figure 14.** Fracture of strand wire stressed and charged showing staircase pattern

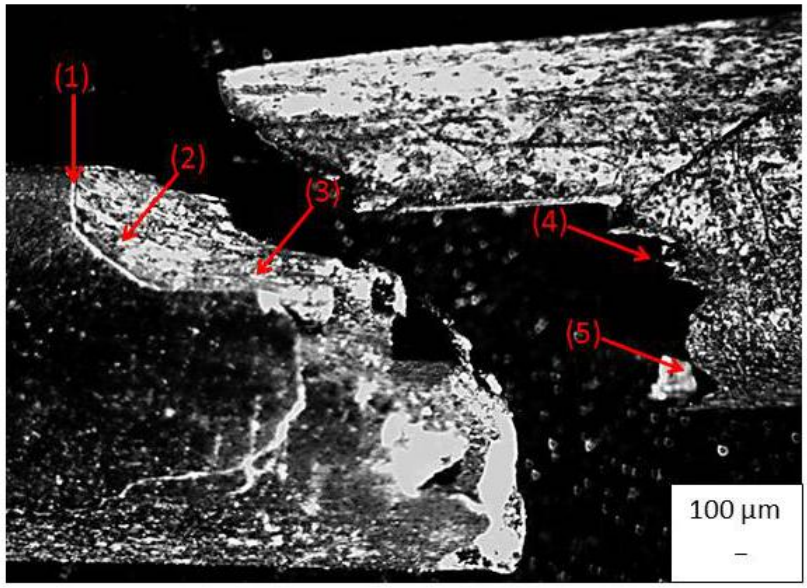


**Figure 15.** Fracture with both sides of the failed wire aligned to show pattern

The similarities between the U-bend specimens at above yield strength values and the stress strand specimens at more realistic stress values show that the level of stress and direction of the stresses applied do not alter the crack propagation pattern shown clearly in the U-bend testing. Also, while the concentration of hydrogen in the charged specimens is high due to the electrochemical charging of the specimens, concentration values within an order of magnitude were measured in strand in which the only source of hydrogen was the surface corrosion on the salted strands in wet ducts. This salted and wet condition can be possible, give an extended time that the strand is left ungrouted.

These experiments suggested that hydrogen embrittlement is a possible mode of failure in stressed strands, and that a measure of caution is in order when exposure severity leads to measured hydrogen levels approaching those observed to make brittle failure possible, albeit in highly severe conditions. It is also noted that the strand material is susceptible to the embrittlement, even when it is not charged to high levels of hydrogen.

## 4. Conclusions

The failure mechanism proposed for stressed cold-worked, pearlitic steel strand under tension follows a multi-step process of surface crack propagation, separation of the lamellae layers, propagation through spaces in layers in staircase manner, and loss of the cross-section through bond breaking to point of ductile overload.

While the steel strand under stress may be susceptible to HE, it is unlikely a factor for strand left ungrouted for an extended period of time. This is only true for strands in ducts in which water ingress and salt deposition have been mitigated, otherwise over a long period in the ungrouted condition the strands may fail due to HE.

## Acknowledgments

The authors thank the Florida Department of Transportation, as well as the Alfred P. Sloan Foundation for their material support of this study (*The opinions, findings, and conclusions expressed here are those of the author and not necessarily those of any supporting organizations*).

## References


1. ACI (American Concrete Institute) "ACI 222.2R-01, Corrosion of Prestressing Steels - Report by ACI Committee 222." Farmington Hills, MI, 2001.
2. D. G. Enos , and J. R. Scully, “A Critical-Strain Criterion for Hydrogen Embrittlement of Cold-Drawn, Ultrafine Pearlitic Steel”, Metallurgical and Materials Transactions, 2002, Volume 33A, Pages 1-16.
3. D. A. Jones, “Principles and Prevention of Corrosion”, Second Edition, Prentice Hall, New Jersey, 1996.
4. I. Moro, L. Briottet, P. Lemoine, E. Andrieu, C. Blanc, and G. Odemer, “Hydrogen Embrittlement Susceptibility of a High Strength Steel X80”, Materials Science and Engineering A, July 2010, Volume 527, pages 7252-7260.
5. S. Lynch, “Hydrogen Embrittlement Phenomena and Mechanisms”, Journal of Corrosion Review, 2012, Volume 30, pg. 105-123.
6. J. Mietz, “Investigations on Hydrogen-Induced Embrittlement of Quenched and Tempered Prestressing Steels”, Materials and Corrosion Journal, 2000, Volume 51, pages 80-90.
7. W. H. Hartt, C.C. Kumria, and R.J. Kessler, “Influence of Potential, Chlorides, pH, and Precharging Time on Embrittlement of Cathodically Polarized Prestressing Steel”, Corrosion Journal, May 1993, Volume 49, Number 5, pages 377-385.
8. R. A. Oriani, “The Physical and Metallurgical Aspects of Hydrogen in Metals”, Fourth International Conference on Cold Fusion, 1993.
9. D. G. Enos, A. J. Williams, G. G. Clemeña, and J. R. Scully, “Impressed-Current Cathodic Protection of Steel-Reinforced Concrete Pilings: Protection Criteria and the Threshold for Hydrogen Embrittlement”, Corrosion, May 1998, Volume 54, Number 5, Pages 389-402.
10. J. Fernandez, “Stress corrosion cracking of high strength stainless steels for use as strand in prestressed marine environment concrete construction: SCC of high strength SS for use as strand”, Material and Corrosion Volume 66, Pages 1269–1278, April 2015.
11. A. A. Sagüés, J. Fernandez, M. Hutchinson, and G. Mullins,” Corrosion Characteristics of Unprotected Post-Tensioning Strands Under Stress “, Florida Department of Transportation BDJ84 977-22, May 2014.